Asymmetric Modes and the Transition to Vortex Structures in Rotating Rayleigh-Bénard Convection

Fang Zhong, Robert Ecke, and Victor Steinberg[a]

Physics Division and Center for Nonlinear Studies, Los Alamos National Laboratory, Los Alamos, New Mexico 87544

(Received 10 January 1991)

We report heat transport measurements and optical shadowgraph visualization of rotating Rayleigh-Bénard convection. For dimensionless rotation rates $140 < \Omega < 4300$, the initial transition to convection, occurring at a Rayleigh number R much less than the linear-stability value for roll or vortex states, is a forward Hopf bifurcation to an azimuthally asymmetric state with mode number n. States with $n=3$, 4, 5, 6, and 7 exist at low to moderate R and precess with frequencies that depend on R and Ω. At higher R there is a continuous transition to a state with noisy, time-dependent heat transport, a distinct array of vortices in the central region, and a modulation of the precession speed of the outer structures.

PACS numbers: 47.20.−k, 47.25.Ae

The combination of thermally induced buoyancy and of a Coriolis force is fundamental to many problems in geophysical fluid dynamics, in astrophysics, and in the study of nonlinear instabilities involving multiple control parameters. An important question is how turbulent states evolve in these systems. Here we present experimental results for a horizontal layer of fluid heated from below and rotated about a vertical axis, which may be regarded as an idealization of the problems mentioned above. For this case, it is known that convection is suppressed by the rotation, and at large rotation rates heat is predicted to be transported by vortex structures rather than by convection rolls [1,2]. Our experimental results are based on shadowgraph flow visualization and heat transport measurements for a cylindrical sample of radius-to-height ratio $\Gamma=1$. As the temperature difference ΔT is increased quasistatically, the measurements show that for $\Omega=2145$ the conductive state loses stability to a mode of fivefold azimuthal symmetry with amplitude maxima localized near the lateral wall. Modes with fourfold, fivefold, and sevenfold symmetry can also be created by using different time histories of ΔT. We find that the first bifurcation is a Hopf bifurcation to a time-periodic state in which the convective structure precesses in the rotating frame. The spatial symmetry of our pattern agrees qualitatively with a recent linear-stability analysis [3]; but in the theoretical work it was assumed that the structure would be stationary in the rotating frame. An interesting aspect of this instability in the finite system, noticed also in previous heat transport experiments [4,5], is that it occurs at a *smaller* value of ΔT than the predicted value for the infinite system. This contrasts with the usual situation, where finite-size effects stabilize the conduction state.

As ΔT is increased well beyond the first bifurcation point ΔT_c, we find that the maxima of the flow field, which close to onset were localized near the lateral walls, develop spiral arms that reach into the cell interior and, with increasing ΔT, form vortices with an initial spatial arrangement which retains the n-fold symmetry of the states close to onset. Upon further increase of ΔT, the vortex structure becomes aperiodically time dependent and evolves into a turbulent state. This time dependence manifests itself in the heat transport which, at a constant heat current, leads to aperiodicity in ΔT. The rms amplitude of this noise grows continuously from zero at a second bifurcation point which is located approximately at $3.7\Delta T_c$. At the highest values of ΔT, far above onset, the flow is highly turbulent but the vortices persist as coherent spatial structures.

The experiment consists of water at 23.8 °C in a cylindrical convection cell with radius $r=5.0$ cm, height $d=5.0$ cm, and radius-to-height ratio $\Gamma\equiv r/d=1.0$. The boundaries of the cell are thermally insulating Plexiglas sidewalls, a sapphire top plate that is temperature regulated to ± 0.5 mK, and a mirror-polished, nickel-plated copper bottom plate. The bottom plate is heated uniformly with a constant heat current. Time dependence in the heat transport is measured using a thermistor in the center of the bottom plate. Thermal forcing induced by the heat current is measured in terms of the dimensionless Rayleigh number R, proportional to the temperature difference ΔT across the fluid layer. The rotation is parametrized by a dimensionless angular frequency $\Omega \equiv \Omega_D d^2/\nu$, where Ω_D is the angular rotation frequency and ν is the kinematic viscosity. In these measurements a rotation rate $\Omega=2145$ corresponds to a dimensioned angular frequency of $\Omega_D=0.7917$ rad/sec. A reduced bifurcation parameter for this system is defined as $\epsilon\equiv[\Delta T - \Delta T_c(\Omega)]/\Delta T_c(\Omega)$, where $\Delta T_c(\Omega)$ is the critical temperature difference for the onset of convection at a particular Ω.

In addition to R and Ω, other factors can influence the convective flow. The ratio $\Omega_D^2 r/g$ measures the relative importance of centrifugal-to-gravitational forces and is less than 0.01 for the highest rotation rate used in our experiment, $\Omega=4274$, indicating that centrifugal effects should be small [5]. Geometry-dependent effects are also important for small-Γ convection cells. In nonrotating convection the conduction state is stabilized by the lateral walls and for $\Gamma=1$ cylindrical cells the convective flow is axisymmetric. In the rotating case there are two complications: First, in order to obtain the large dimensionless

rotation rates necessary to observe vortex structures (recall that Ω scales as d^2) while minimizing centrifugal contributions and maintaining highly controlled boundary conditions, the convection cell is constrained to have Γ of order 1. Second, the spatial scale for convective structures changes dramatically with Ω so that at $\Omega = 5000$ the critical wave number for the laterally infinite case is about 8 times smaller than at $\Omega = 0$ [1]. Thus, the effective Γ at high Ω is "moderate" rather than "small" as compared to similar nonrotating convection studies. Consequently, for a $\Gamma = 1$ convection cell one would think that at $\Omega = 0$ the onset would be shifted to higher ΔT and would approach the infinite system result for large Ω as the effective Γ increased, thereby reducing the influence of the sidewalls.

The onset of convection and the transition to a noisy time-dependent state are determined from heat transport data, reported in terms of the Nusselt number Nu, the total thermal conductivity normalized by the thermally diffusive part. We concentrate on the rotation rate $\Omega = 2145$, although similar phenomena are observed at other Ω [6]. The data in Fig. 1 show a forward bifurcation to convection [Fig. 1(a)] and a secondary, continuous transition to aperiodic time-dependent convection at $\epsilon \approx 2.7$ [Fig. 1(b)]. Four distinct Nusselt number branches are accessible using different histories of ΔT over a wide range in ϵ [6]. The bifurcation values for the transitions illustrated in Fig. 1 are determined from heat transport data for different rotation rates and are plotted in Fig. 2. The onset values, shown in Fig. 2 by open circles, are substantially below the values expected from linear-stability analysis of the usual convection planforms of rolls, hexagons, or squares (the vortex state can be described as a smooth transformation of the cellular states) for $\Gamma = \infty$ [1,2]. They are in semiquantitative agreement with experimental heat transport measurements in helium [5] and in water [4] for various Γ values. This is unexpected from the usual understanding of the effect of small Γ. Neither finite amplitude instability nor centrifugal effects, however, can account for the observed decrease in onset values [5]. A recent linear-stability calculation [3] showed that azimuthally asymmetric modes localized near the lateral walls can have substantially lower onset values relative to those determined for the infinite system. The predictions of linear-stability calculations are illustrated in Fig. 2 for a laterally infinite system and for a cylindrical cell with $\Gamma = 1.0$ for both perfectly conducting and perfectly insulating sidewalls. The data are in qualitative agreement with the finite-geometry calculations, but no visualization of the convection pattern had been done in the previous experiments [4,5].

Using shadowgraph visualization we find that the four different branches in Fig. 1 correspond to four different convective modes consistent with the finite-geometry calculations [3]. Their convective motion is localized near the lateral boundary with azimuthal periodicity, $e^{in\theta}$, with

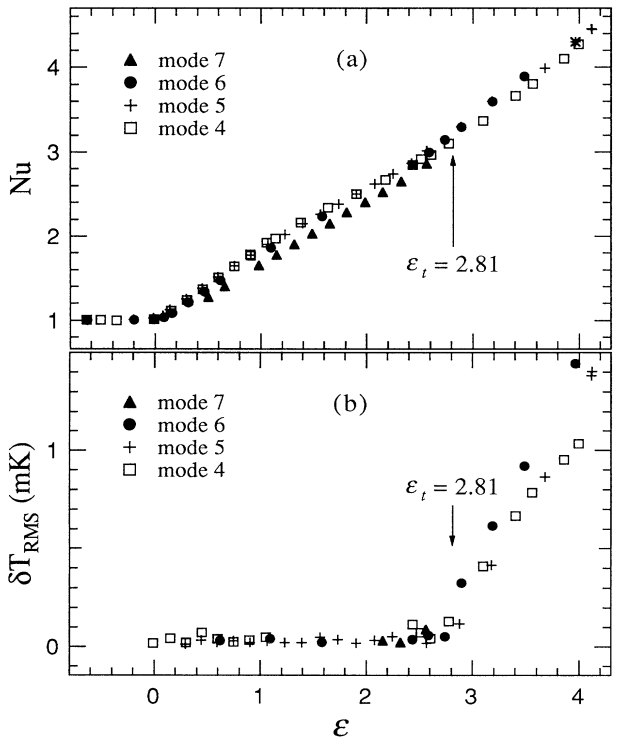

FIG. 1. (a) Nusselt number vs ϵ at $\Omega = 2145$ for states with the mode numbers 4 (□), 5 (+), 6 (●), and 7 (▲). The transition to noisy time dependence for mode 5 is indicated by a vertical arrow at $\epsilon_t = 2.81$. (b) rms temperature fluctuations $\delta T_{\rm rms}$ in the bottom plate vs ϵ, showing the transition to noisy time dependence. Data for different mode numbers are labeled as in (a).

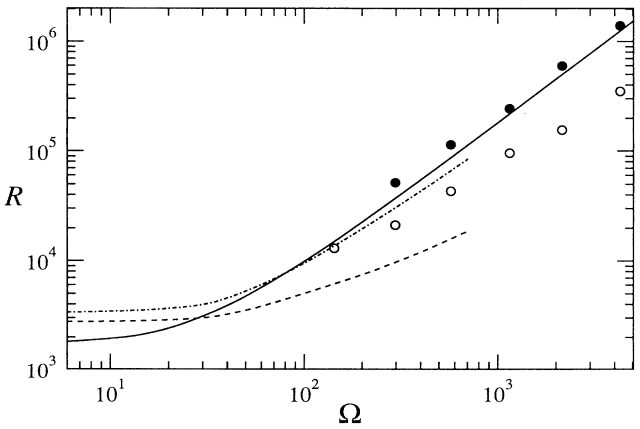

FIG. 2. Stability diagram in R vs Ω parameter space. The solid line shows the prediction of linear-stability calculations for the laterally infinite system and the broken lines indicate linear analysis for asymmetric states in a $\Gamma = 1$ cylindrical container with insulating (---) and conducting (-·-·) sidewall boundary conditions (after Ref. [3]). The data show the convective onset (○) and the onset of noisy time dependence (●).

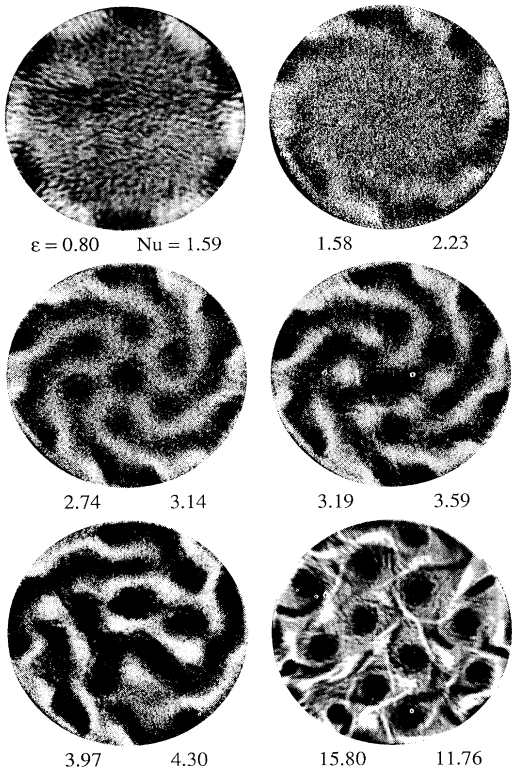

FIG. 3. Shadowgraph images for $\Omega = 2145$ showing evolution of the convective state with increasing ϵ. Mode 6 is the azimuthal mode number for states with $\epsilon < 3.2$. For $\epsilon = 3.97$ there has been a transition to a mode-5 state. Values of ϵ and the Nusselt number are shown for each pattern.

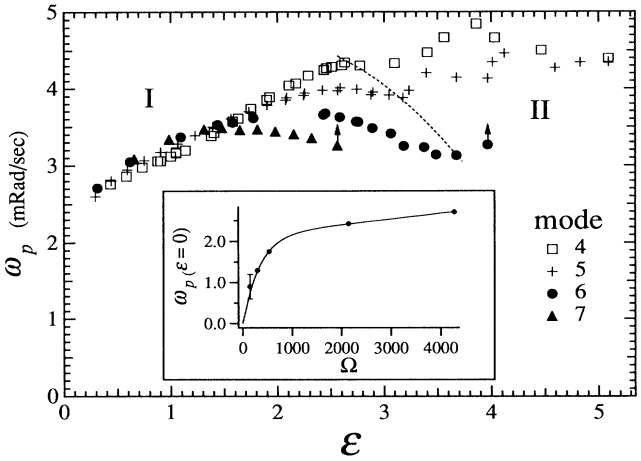

FIG. 4. Azimuthal precession frequency ω_p vs ϵ for $\Omega = 2145$ for different modes labeled $n = 4$ (□), 5 (+), 6 (●), and 7 (▲). Inset: $\omega_p(\epsilon = 0)$ vs Ω.

$n = 4$, 5, 6, and 7. If ΔT is increased slowly, the state that forms has $n = 5$, whereas the other modes have slightly higher onset values and are reached by history-dependent changes in ΔT [6]. The first pattern in Fig. 3 illustrates the convective structure for an $n = 6$ state at $\epsilon = 0.80$ (dark regions are warm upflow and bright regions are cold downflow). An interesting and unexpected feature of the experimental asymmetric states is that they precess in the rotating frame counter to the direction of rotation. The precession frequency and the direction of the precession relative to the rotation direction do not change when the sense of rotation is reversed and asymmetries or imperfections in the cell do not appear responsible for the precession since properties of the precession are quantitatively repeatable, even after numerous modifications of the sample cell with different top-bottom plates and lateral walls. One of these properties, the angular precession velocity $\dot{\theta}_n$, is determined for each mode by plotting a space-time graph of the azimuthal intensity near the outer boundary versus angle. The precession frequency, $\omega_p = 2\pi r\dot{\theta}_n/\lambda = \dot{\theta}_n n$, where $\lambda = 2\pi r/n$, is about 800 times less than Ω_D at $\Omega = 2145$ and does not depend strongly on n for small ϵ (see Fig. 4). In region I, only a single frequency and its harmonics are seen, whereas in region II, the precession is strongly modulated. Although the secondary bifurcations that produce the modulated precession have not been studied in detail, quasiperiodic and chaotic wave states have been observed for different values of ϵ and Ω and are the mechanism for conversions between different modes, indicated by arrows in Fig. 4.

It is important to determine if the precessing state persists down to the convective onset. The patterns in our cell cannot be visualized if $\epsilon < 0.3$, but because the patterns precess, the mode number and the precession frequency can be determined to much smaller ϵ by two local temperature probes embedded in the lateral walls at a fixed angular orientation. The frequency is determined from the time series of either probe and the mode number is determined from the phase difference between the signals at the separate probes. The $n = 5$ state is found to be the preferred state at onset for $\Omega = 2145$ and 4274, $n = 4$ is favored for $290 < \Omega < 1100$, and $n = 3$ is chosen for $\Omega = 142$. The mode number selected in the experiment is systematically larger than that predicted in the linear-stability calculations [3]. We also find that the precesssion frequency ω_p of the onset mode varies linearly with ϵ and intercepts a finite value at $\epsilon = 0$. In addition, the amplitude of the precessing wave has the square-root dependence characteristic of a Hopf bifurcation. These data indicate that the initial bifurcation to convection is a Hopf bifurcation, with the rotation breaking azimuthal reflection symmetry and selecting one direction of wave propagation [7]. It would be useful, therefore, to recalculate the finite-Γ, linear-stability problem without assuming time-independent solutions. Such calculations might resolve the quantitative discrepancies in onset mode number between theory and experiment. Other explanations for the precession, based on centrifugal effects, are ruled out by the $\Omega \rightarrow -\Omega$ symmetry, the Hopf-like depen-

dence of the amplitude and frequency of the traveling wave, and the sharpness of the onset of convection. In addition, the variation of ω_p with Ω (see the inset of Fig. 4) is consistent with the linear dependence for small Ω expected for a Hopf bifurcation with rotation-induced broken reflection symmetry [7].

As ϵ increases, the wall structures grow into the interior of the cell. In Fig. 3 we show a series of patterns for increasing ϵ. A localized wall state with $n=6$ and at $\epsilon=0.8$ is shown first. At $\epsilon=1.58$ the wall structures extend noticeably into the interior region and leading spirals are formed. At $\epsilon=2.43$ (not shown), this spiral structure fills the entire cell and the change in slope of the Nusselt number occurs at about this ϵ. Vortices then start to form in the central region at the end of the spirals until, at $\epsilon=2.74$, a regular hexagonal cell of vortices is fully established [8]. The symmetry of the arrangement of the interior vortices is the same as the n-fold periodicity of the wall structures. The same behavior is seen for higher Ω up to 4274, but with smaller vortex size, smaller hexagon structure, and smaller spiral widths [6]. For $\epsilon > 2.74$ aperiodic time dependence is measured in the heat transport [see Fig. 1(b)]. For successively larger ϵ the regular structure becomes more and more dynamic; at $\epsilon=15.80$ the dark regions (vortices) propagate rapidly, undergoing vigorous collisions and interactions. Although the flow is strongly turbulent, the individual vortices retain a definite coherent structure. Details on Ω's other than the value of 2145, on the complicated structure of the precession modulation and the related mode conversions, and on the dynamics of the thermally driven vortex structures are discussed elsewhere [6].

We would like to acknowledge valuable assistance from Timothy Sullivan, helpful advice from Guenter Ahlers, and useful discussions with Mike Cross, Rick Goldstein, Edgar Knobloch, Manfred Lucke, Mary Silber, and Thierry Passot. This work was supported by DARPA/ACMP Contract No. DPP88-50.

[a]Permanent address: Weizmann Institute of Science, 76 100 Rehovot, Israel.

[1] S. Chandrasekhar, *Hydrodynamic and Hydromagnetic Stability* (Dover, New York, 1961).

[2] G. Veronis, J. Fluid Mech. **5**, 401 (1958).

[3] J. C. Buell and I. Catton, Phys. Fluids **26**, 892 (1983).

[4] H. T. Rossby, J. Fluid Mech. **36**, 309 (1969).

[5] J. M. Pfotenhauer, J. J. Niemela, and R. J. Donnelly, J. Fluid Mech. **175**, 85 (1987); includes a thorough discussion of finite amplitude and centrifugal effects in rotating Rayleigh-Bénard convection.

[6] F. Zhong, R. E. Ecke, and V. Steinberg (to be published).

[7] E. Knobloch (private communication). Because the unperturbed state ($\Omega=0$) does not precess there is only a single state in the rotating case instead of the usual left-right traveling-wave pair associated with a complex-conjugate pair of eigenvalues.

[8] Although vortex structures were observed for a rotating convection with a free upper surface, it was not known whether such states exist when the upper surface is bounded and isothermal: Y. Nakagawa and P. Frenzen, Tellus **7**, 1 (1955); B. M. Boubnov and G. S. Golitsyn, J. Fluid Mech. **167**, 503 (1986).

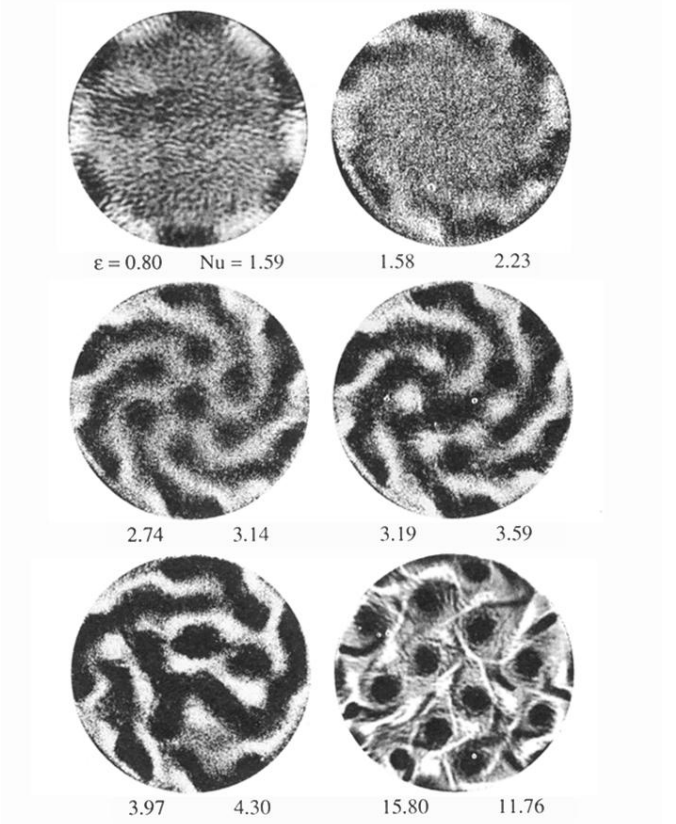

FIG. 3. Shadowgraph images for $\Omega = 2145$ showing evolution of the convective state with increasing ϵ. Mode 6 is the azimuthal mode number for states with $\epsilon < 3.2$. For $\epsilon = 3.97$ there has been a transition to a mode-5 state. Values of ϵ and the Nusselt number are shown for each pattern.